Check for updates

Geophysical Research Letters

RESEARCH LETTER
10.1029/2023GL105066

The Lasting Legacy of Megaflood Boulder Deposition in Mountain Rivers

S. M. Morey[1,2], C. M. Shobe[3,4], K. W. Huntington[1], K. A. Lang[5], A. G. Johnson[1], and A. R. Duvall[1]

[1]Department of Earth and Space Sciences, University of Washington, Seattle, WA, USA, [2]Cooperative Institute for Research in Environmental Sciences, University of Colorado, Boulder, CO, USA, [3]Department of Geology and Geography, West Virginia University, Morgantown, WV, USA, [4]U.S. Forest Service, Rocky Mountain Research Station, Fort Collins, CO, USA, [5]School of Earth and Atmospheric Sciences, Georgia Institute of Technology Main Campus, Atlanta, GA, USA

Key Points:

- We studied channel response to megaflood boulder deposition in the eastern Himalaya using a numerical model
- Megaflood boulder deposition locally changes channel steepness up to 180%, creating >100 knickpoints
- The compounding effect from multiple megaflood boulder deposits in rapid succession perturbs channel form for many thousands of years

Supporting Information:

Supporting Information may be found in the online version of this article.

Correspondence to:

S. M. Morey and K. W. Huntington, susannah.morey@colorado.edu; kate1@uw.edu

Citation:

Morey, S. M., Shobe, C. M., Huntington, K. W., Lang, K. A., Johnson, A. G., & Duvall, A. R. (2024). The lasting legacy of megaflood boulder deposition in mountain rivers. *Geophysical Research Letters*, *51*, e2023GL105066. https://doi.org/10.1029/2023GL105066

Received 19 JUN 2023
Accepted 27 NOV 2023

© 2023 The Authors.
This is an open access article under the terms of the Creative Commons Attribution-NonCommercial License, which permits use, distribution and reproduction in any medium, provided the original work is properly cited and is not used for commercial purposes.

Abstract Infrequent, large-magnitude discharge (>10^6 m^3/s) outburst floods—megafloods—can play a major role in landscape evolution. Prehistoric glacial lake outburst megafloods transported and deposited large boulders (≥4 m), yet few studies consider their potential lasting impact on river processes and form. We use a numerical model, constrained by observed boulder size distributions, to investigate the fluvial response to boulder deposition by megaflooding in the Yarlung-Siang River, eastern Himalaya. Results show that boulder deposition changes local channel steepness (k_{sn}) up to ∼180% compared to simulations without boulder bars, introducing >100 meter-scale knickpoints to the channel that can be sustained for >20 kyr. Simulations demonstrate that deposition of boulders in a single megaflood can have a greater influence on k_{sn} than another common source of fluvial boulders: incision-rate-dependent delivery of boulders from hillslopes. Through widespread boulder deposition, megafloods leave a lasting legacy of channel disequilibrium that compounds over multiple floods and persists for millennia.

Plain Language Summary Megafloods (discharge equivalent to ≥400 instantaneously draining Olympic-sized swimming pools per second) can transport a lot of material, including car- to house-sized boulders. Because these boulders are so big, they remain in the channel until the next megaflood or until they weather into smaller pieces. We use a computer model to understand the impact of these megaflood deposited boulders on mountain river processes. We find that megaflood boulders can protect the river from being eroded, causing other processes, like tectonic uplift, to outcompete erosion. Megaflood boulders cause small steps to form within the river. Our modeling shows that these effects can be felt for >20,000 yrs after a single flood. We suggest that megaflood deposition (in addition to erosion) can cause a significant, unique change in mountain river processes.

1. Introduction

High-magnitude, low-frequency geomorphic events, such as large floods and landslides, perturb landscapes and cause long-lasting geomorphic disequilibrium. For instance, megafloods (>10^6 m^3/s) sourced from the failure of dammed lakes have been shown to dramatically alter the topography they inundate (Baker & Milton, 1974; Bretz, 1925; Gilbert, 1890; O'Connor et al., 2013). Quantifying the amount, rate, and mechanisms of erosion has been a primary focus of megaflood research (Baker & Kale, 1998; Lang et al., 2013; Larsen & Lamb, 2016). However, megafloods and other high discharge outburst floods can also deposit immense volumes of sediment throughout the flood pathway, including very coarse sediment like boulders 4–20 m in diameter (hereafter, "coarse boulders" refers to any sediment >4 m in diameter).

The introduction of coarse boulders into mountain river channels may inhibit erosion by increasing hydraulic roughness and armoring the channel bed (Cook et al., 2018; Schneider et al., 2015; Shobe et al., 2016; Shobe, Bennett, et al., 2021; Shobe, Turowski, et al., 2021; Sklar & Dietrich, 2004). Boulder-driven erosion resistance can create knickpoints that can be sustained for 10^1–10^4 years (e.g., Hewitt, 1998; Korup, 2006; Korup et al., 2006; Ouimet et al., 2007; Pratt-Sitaula et al., 2004). These findings suggest that megafloods have the potential to leave a long-lived imprint on river form through widespread, geologically instantaneous boulder deposition in otherwise rapidly eroding rivers. The magnitudes and timescales of river response to megaflood deposition have not been quantified.

19448007, 2024, 1, Downloaded from https://agupubs.onlinelibrary.wiley.com/doi/10.1029/2023GL105066, Wiley Online Library on [27/12/2023]. See the Terms and Conditions (https://onlinelibrary.wiley.com/terms-and-conditions) on Wiley Online Library for rules of use; OA articles are governed by the applicable Creative Commons License

In this paper, we present numerical modeling results that quantify the geomorphic legacy of megaflood boulder deposits, using the Yarlung-Siang River (YSR) in the eastern Himalaya as a case study. Informed by >10,000 boulder measurements on the YSR, we modify an existing river profile evolution model (Shobe et al., 2016, 2018; Shobe, Bennett, et al., 2021) to elucidate how the extreme sizes of megaflood-derived boulders as well as the regionally synchronous nature of boulder deposition influence the post-megaflood evolution of the YSR river profile (Figure 1). In general, we expect that megaflood boulder delivery will result in localized surface uplift of the riverbed driven by rock uplift that outpaces boulder-inhibited erosion. We hypothesize that the morphologic response to megaflood boulder deposition will (a) be greater in magnitude and (b) have a unique signature relative to that of the incision-rate-dependent delivery of hillslope-derived boulders to a bedrock river channel that might be expected in a rapidly eroding landscape in the absence of megafloods (e.g., Attal et al., 2015; Shobe et al., 2016). While we are inspired by megafloods on YSR in the eastern Himalaya, we expect the results to be applicable to any event that can lead to synchronous widespread deposition of large, immobile boulders in mountain regions (e.g., earthquake-triggered regional landsliding).

2. Eastern Himalayan Megafloods

The YSR in the eastern Himalaya (Figure 1) provides an interesting case study to examine the impact of widespread megaflood- or event-deposited boulders because of its history of outburst floods and high concentrations of related coarse boulders in the channel. Throughout the late Pleistocene and early Holocene, the YSR experienced outburst megafloods sourced from glacially impounded lakes with estimated volumes up to 80–800 km^3. Estimates from paleolake deposits (Liu et al., 2015; Montgomery et al., 2004; Song et al., 2013; Xu et al., 2020), moraine dams (Figure 1, Montgomery et al., 2004), and slackwater flood deposits (Borgohain et al., 2020; Lang et al., 2013; Panda et al., 2020; Srivastava & Misra, 2012; Srivastava et al., 2017; Turzewski et al., 2020) indicate that multiple megafloods originated from glacially impounded lakes at or upstream of the Namche Barwa massif (Figure 1). Outburst megafloods resulting from the failure of dams at the Namche Barwa massif coursed down the YSR, and preliminary observations of the eastern Himalayan megaflood pathway identified >70 boulder bars that contain coarse boulders too large to be regularly moved by modern meteoric discharges (Morey et al., 2022; Turzewski et al., 2019). In the YSR, we observe evidence that many boulder bars are megaflood-derived, including large (>4–10 m diameter) imbricated boulders that are rounded on all sides (Figures 1d–1f). On at least one such bar, coarse boulders are of a different lithology than the local bedrock on which they are deposited (Figures 1d and 1e). While some of the coarse boulder bars identified could have been deposited by local landsliding rather than megaflooding, most observed boulder bars contain grains that could only be moved by outburst megafloods (Morey et al., 2022).

Megaflood boulder bars are unique compared to typical hillslope-derived boulder deposits because they are deposited synchronously and regionally throughout the flood pathway. There is also reason to believe that loci of boulder deposition may remain consistent over multiple megafloods. Two-dimensional hydraulic modeling of a glacial lake outburst megaflood (Morey et al., 2022) on the YSR indicates that high-relief valley topography exerts a primary control on flood hydraulics and subsequent depositional patterns. This means that the spatial distribution of megaflood boulder bar deposits may differ from boulder bars deposited by meteoric flooding (i.e., monsoon flooding) or those produced from typical channel-hillslope interactions (i.e., boulders like those described in Shobe et al., 2016), and further that repeated megafloods may deposit coarse boulders in the same locations. These unique characteristics of megaflood boulder bars suggest that megaflood-derived boulders might have a different long-term legacy in mountain rivers compared to boulders deposited through other processes. While deposition of any large boulders in a bedrock channel locally reduces erosion rates, which causes the channel to steepen (Ouimet et al., 2007; Shobe et al., 2016, 2018; Shobe, Turowski, et al., 2021), we assess here the extent to which megaflood boulder deposition leaves a distinctive imprint on mountain rivers.

3. Methods

We modify a 1D numerical model, that calculates the erosion-inhibiting effects of infrequently mobile boulders along a river's longitudinal profile (Shobe et al., 2016, 2018; Shobe, Bennett, et al., 2021), to assess post-megaflood erosion dynamics in a modeled mountain river scaled to the YSR. The model accounts for two key effects of immobile boulders in the channel: armoring that shields the bed from erosion, and hydraulic drag that reduces erosive stresses on the bed. Once a boulder is in the channel, it can degrade via abrasion and move

10.1029/2023GL105066

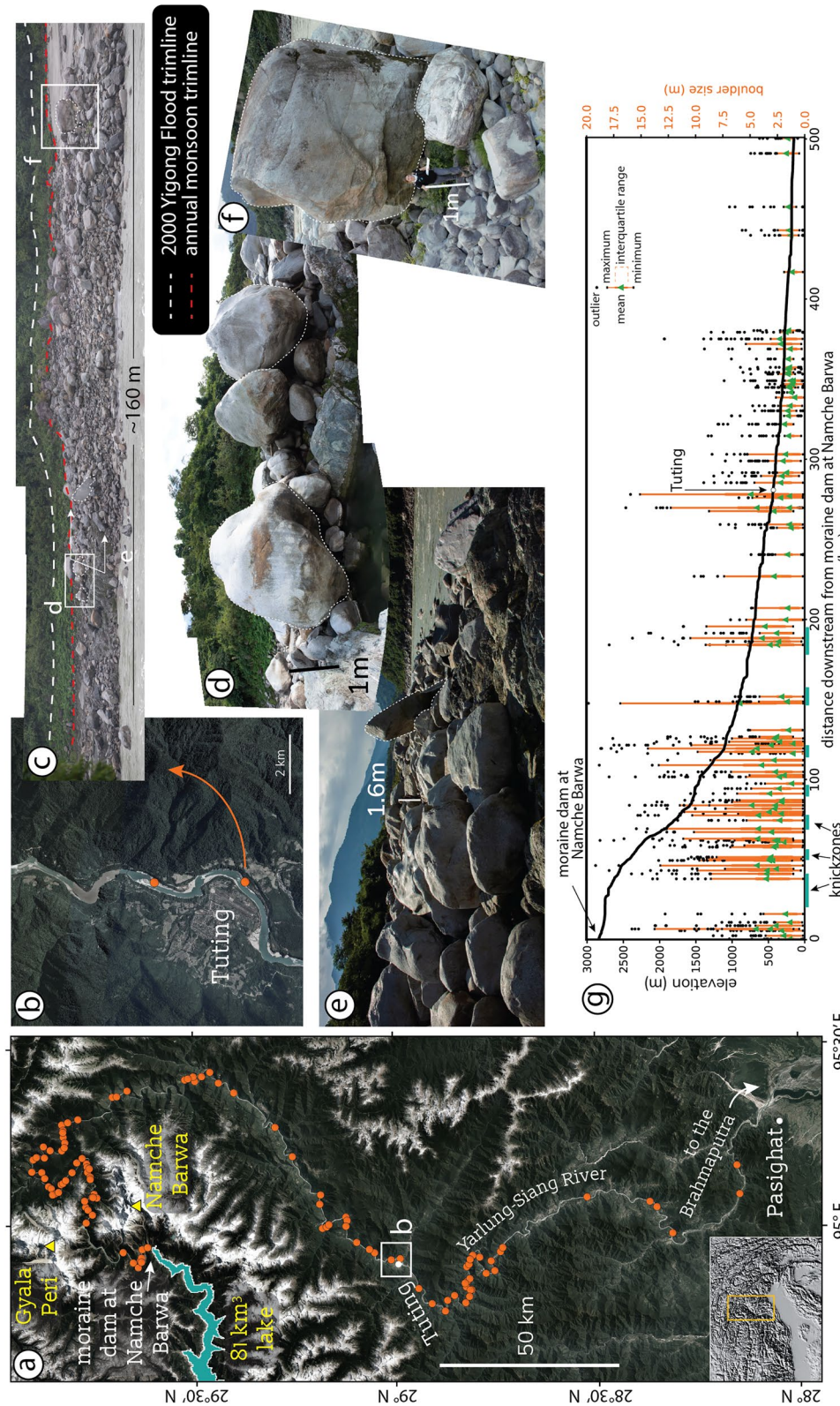

Figure 1. (a) Regional map of the Yarlung-Siang River (YSR) between observed megaflood dams at Namche Barwa and where the YSR exits the range to join the Brahmaputra River at Pasighat. Orange dots represent observed boulder bars (b) Tuting area (c) a boulder bar at Tuting (d–f) boulders on the bar from (c), (g) The longitudinal profile of the YSR with the grain size distribution of boulder measurements that are ≥2 m at each observed boulder bar.

19448007, 2024, 1, Downloaded from https://agupubs.onlinelibrary.wiley.com/doi/10.1029/2023GL105066, Wiley Online Library on [27/12/2023]. See the Terms and Conditions (https://onlinelibrary.wiley.com/terms-and-conditions) on Wiley Online Library for rules of use; OA articles are governed by the applicable Creative Commons License

19448007, 2024, 1, Downloaded from https://agupubs.onlinelibrary.wiley.com/doi/10.1029/2023GL105066, Wiley Online Library on [27/12/2023]. See the Terms and Conditions (https://onlinelibrary.wiley.com/terms-and-conditions) on Wiley Online Library for rules of use; OA articles are governed by the applicable Creative Commons License

via sliding if there is sufficient shear stress to mobilize it. For simplicity, we neglect bedload and suspended load sediment dynamics. Model runs are inspired by the YSR, so the model domain encompasses a 500 km stretch of the YSR longitudinal profile, with imposed relationships among downstream distance, drainage area, and river width that are broadly reflective of the YSR (see Supporting Information S1 for detailed model methods).

3.1. Initial and Boundary Conditions

The initial condition is a steady-state river profile generated to roughly match the length and fluvial relief of the YSR between the moraine dam at Namche Barwa (Figure 1) and where the YSR exits the mountains to join the Brahmaputra River (Figure 1a). The upstream extent of the model domain is restricted to the YSR downstream of the moraine dam (Figure 1a)—the same location as the megaflood dam in Morey et al. (2022). We assume a constant rock uplift rate of 0.001 m/yr, similar to typical eastern Himalayan exhumation rates that characterize much of the flood pathway (e.g., Lang et al., 2016), and a concavity of 0.8 is calculated for the equilibrium channel profile and is used as the reference concavity for later calculations (Fig. S1). River width follows a power-law function of drainage area (e.g., Wohl & David, 2008); downstream width increases were constrained by width measurements from satellite imagery at the upstream and downstream ends of the study reach. We derive the spatial distribution of megaflood boulder bars, as well as the size distribution of the boulders in each bar, from new measurements of boulder size distributions from satellite imagery of 106 in-channel boulder bars interpreted to be associated with megaflood deposition by us and by previous studies (Figures 1a and 1g, Morey et al., 2022; Turzewski et al., 2019). River discharge is modeled using a Weibull distribution with parameters appropriate to monsoon-influenced Eastern Himalayan rivers (Scherler et al., 2017). We track bed elevation (bedrock surface not including any boulders), channel steepness (k_{sn}), the number and size of boulders, and the fraction of the bed covered by boulders at a grid spacing of 250 m along the river profile.

3.2. Experimental Design

We compare four experiments to examine the influence of megaflood-deposited boulders on subsequent channel evolution. All four scenarios (R1–R4) were run over 20 kyr with timesteps of 1 year beginning from the equilibrium longitudinal profile described in 3.1. R1 is a control scenario. It involves no boulder delivery to the river by any mechanism. R2 is a run with exclusively hillslope-derived boulders that represents a system that does not experience megaflood boulder deposition. This run mimics the experimental set up from Shobe et al. (2016), in which hillslopes deliver boulders to the channel at a rate proportional to the rate of river incision (see Supporting Information S1 for details of model setup). In R2, hillslope-derived boulders have a uniform size of 4 m. R3 uses observed measurements of boulder size from the YSR to simulate the impact of boulders deposited in a single megaflood. Boulders are "deposited" in the first timestep in bars, the locations of which are taken from remote observations of 106 megaflood boulder bars in the YSR (discussed below, Figure 1). In R4, the spatial distribution is the same as in R3, but all boulders are 4 m in diameter—the hypothesized upper limit of what modern flows could potentially mobilize (Morey et al., 2022). This final scenario allows us to disentangle the impact of the spatial distribution of boulder deposition style from the impact of grain size.

In addition to the 76 bars identified in Turzewski et al. (2019) and Morey et al. (2022), we identify a further 30 boulder bars that are below monsoon inundation levels in the YSR and contain boulders too coarse to move in modern annual flows. We made measurements of roughly 100 individual boulders within each bar using Google Earth imagery. Uncertainty was estimated by comparing measurements to structure from motion (SfM) photogrammetry from one bar (Figure 1c; see Supporting Information S1 for detailed methods). For boulders >2 m, there is a maximum compounded error between the two measurements of 0.3 m (Table S1 in Supporting Information S1). We scaled the model cell length to the average length of bars (250 m) and determined the cover fraction of each boulder bar deposit by calculating the percent of the monsoon-inundated channel covered by the bar. We determined how many boulders to add at each location based on cover fraction and the 100-measurement grain size distribution. This resulted in 106 unique boulder deposits that cover some fraction of one cell, each at their measured distance downstream of the moraine dam (Figure 1). Simulations of megaflood hydraulics (Morey et al., 2022) indicate that megafloods can mobilize boulders at least 4 m in diameter throughout the eastern Himalayan megaflood pathway. Because we are interested in exceptionally coarse boulders that cannot be moved in annual monsoon floods, we excluded boulders smaller than 4 m in R3. The number and size of boulders in each cell is tracked for each output timestep. We assess the impact of boulder deposition on the river's longitudinal

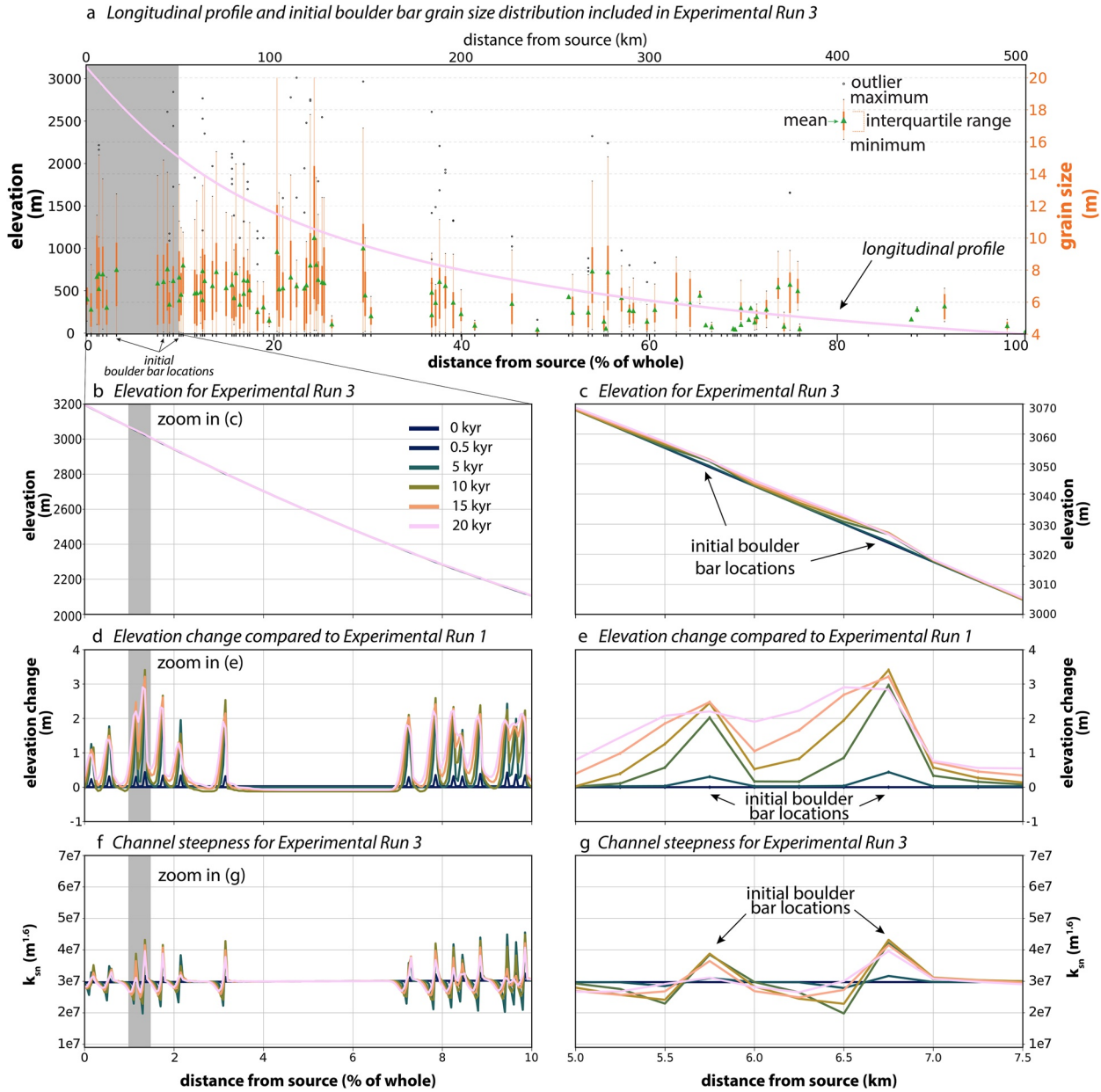

Figure 2. (a) Experimental Run 3 results of the longitudinal profile with initial grain size distributions shown. (b, c) elevation (m) (d, e) elevation change (m) (f, g) channel steepness (k_{sn}), calculated with a fixed concavity of 0.8.

profile through time by calculating the percent difference in profile-averaged k_{sn} for R2, R3, and R4 relative to the same river experiencing no boulder delivery (R1). This value is calculated locally for each cell along the profile (Figure 2) and then local values are averaged over the entire longitudinal profile to obtain an average local percent change in k_{sn} (Figure 3).

4. Results

Boulders sourced from both hillslopes and megafloods reduce erosion rates where they are deposited, allowing rock uplift to outpace river incision, but the scale of elevation change from megaflood boulders (R3) is about an order of magnitude greater than that from hillslope-derived boulders (R2). We observe local, meter-scale changes in elevation that manifest as individual knickpoints at the reach scale but are not visible at the scale of the entire longitudinal profile with its 3,000 m of total fluvial relief (Figures 2a and 2b). In R3, boulders cover a maximum

19448007, 2024, 1, Downloaded from https://agupubs.onlinelibrary.wiley.com/doi/10.1029/2023GL105066, Wiley Online Library on [27/12/2023]. See the Terms and Conditions (https://onlinelibrary.wiley.com/terms-and-conditions) on Wiley Online Library for rules of use; OA articles are governed by the applicable Creative Commons License

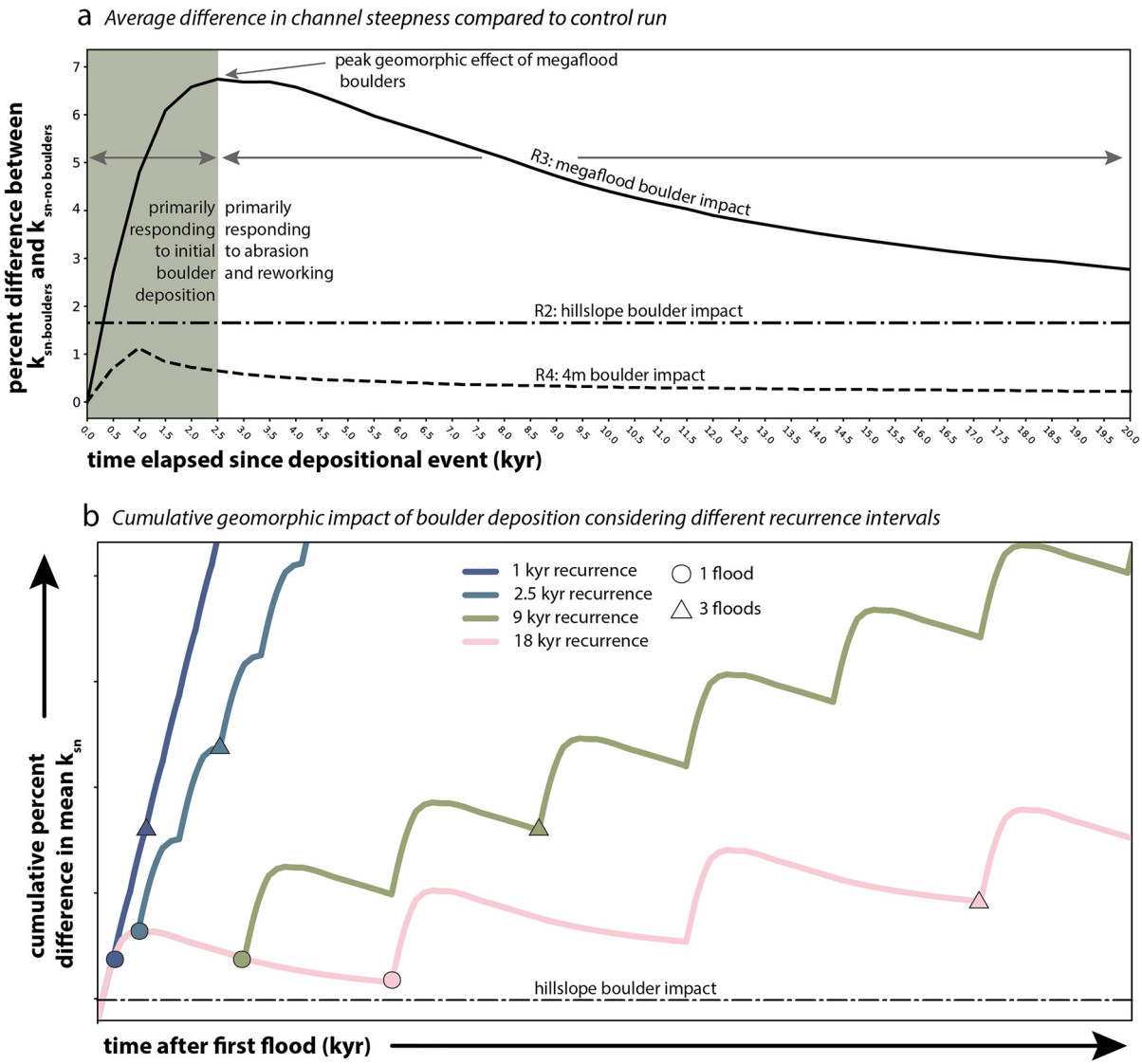

Figure 3. (a) Average local percent change in k_{sn} between R2, R3, and R4 with respect to the baseline at each time-step of the model run as a function of time elapsed after the megaflood depositional event (b) Schematic of cumulative geomorphic impact due to the addition of megaflood boulders from sequences of many floods with four different recurrence intervals: 1, 2.5, 9, and 18 kyr. The dashed line is the same dashed line from (a)—the equilibrium effect of a landscape that experiences hillslope-derived boulder deposition.

of 44% of the channel bed at any given location along the longitudinal profile (a realistic cover percent based on observations), which drives up to 3.5 m of elevation change at each boulder bar over the 20 kyr run (Figures 2c and 2d). Boulder bars from R4 only cause ~1 m of elevation change at each bar location (Figure S4 in Supporting Information S1).

Bars exert a zone of influence both up- and downstream of their initial locations that grows with time as the channel bed adjusts to the presence of boulders. The largest boulders move downstream <500 m during R3 after degrading to smaller sizes that allow transport. As expected, the smaller the initial boulder size, the quicker subsequent transport happens. As boulders degrade to sizes able to move downstream under the imposed discharge distribution, the area that experiences suppressed erosion rates spreads to downstream locations that receive the transported boulders. This effect is enhanced when two boulder bars are close to each other and their zones of influence begin to interact (Figures 2b and 2c). Boulder bars that retain the most megaflood-deposited boulders are those that have boulder bars upstream of them. Winnowed boulders from the upstream bar are transported downstream but get "stuck" at the downstream bar: a boulder that could have been moved at that bar at the

19448007, 2024, 1, Downloaded from https://agupubs.onlinelibrary.wiley.com/doi/10.1029/2023GL105066, Wiley Online Library on [27/12/2023]. See the Terms and Conditions (https://onlinelibrary.wiley.com/terms-and-conditions) on Wiley Online Library for rules of use; OA articles are governed by the applicable Creative Commons License

19448007, 2024, 1, Downloaded from https://agupubs.onlinelibrary.wiley.com/doi/10.1029/2023GL105066, Wiley Online Library on [27/12/2023]. See the Terms and Conditions (https://onlinelibrary.wiley.com/terms-and-conditions) on Wiley Online Library for rules of use; OA articles are governed by the applicable Creative Commons License

beginning of the run now requires more shear stress to move because that downstream bar has decreased the slope at its upstream edge. In R4, because boulders are smaller, they are able to move through the system quicker than boulders in R3. This causes the number of boulders at each location to increase compared to R3 (Figure S4 in Supporting Information S1). However, the smaller size of the R4 boulders means the amount of influence they have is small compared to megaflood-deposited boulders of R3. How long boulder-induced knickpoints remain fairly stationary versus beginning to migrate upstream depends on the river's ability to adjust to the influx of coarse sediment, which is a function of the interactions between discharge, channel width, channel cover fraction, and deposited boulder sizes. We observe in these experiments that the farther downstream a bar is, the earlier knickpoints it creates begin to migrate.

Boulder-induced changes in elevation lead to an increase in k_{sn} immediately downstream of the locus of boulder deposition and a decrease in k_{sn} immediately upstream (Figures 3f and 3g). We assess the impact of boulder deposition on the river's longitudinal profile through time by calculating the average local percent change in k_{sn} compared to the baseline, no boulders run (R1). We then plot the average local percent change for the entire longitudinal profile for each time-step in Figure 3. Megaflood boulders (R2) cause local k_{sn} to change up to 174% with a maximum mean percent change of 6.8% compared to R1 (at 2.5 kyr; Figure 3). 4 m boulders instantaneously deposited in the same locations (R4) cause a maximum change in local k_{sn} of 104%, but only produce a mean percent change of 1.1% (at 1 kyr; Figure 3). Hillslope-derived boulders (R2) only cause k_{sn} to change up to 30% with a mean percent change of 1.7% (Figure 3). Although the peak impact at every bar and location might not occur simultaneously, the average percent change allows us to make interpretations about the influence that widespread megaflood deposited boulder bars have on the whole river reach profile.

5. Discussion

After a megaflood, the river does not return to a smooth, equilibrium profile, even after 20,000 years. While this exact timescale and magnitude of change in k_{sn} depend on our model parameters (e.g., bedrock vs. boulder erodibility), the shape of the megaflood boulder impact curve is revealing (Figure 3). By 500 years, under our imposed boulder size distributions, megaflood boulder deposition has changed k_{sn} more than is possible in a channel with only hillslope-derived boulders (Figure 3a). Megaflood-deposited boulder bars reach their peak impact on the river 2,500 years after deposition (time to peak boulder impact, t_{pbi}). Before t_{pbi}, the river is primarily responding to the boulder deposition by steepening as rock uplift outpaces erosion in boulder-mantled reaches. After t_{pbi}, the river's response is defined by relaxation toward its pre-megaflood state at a rate set by how efficiently it can abrade and transport the boulders and resume bedrock incision. After t_{pbi}, the average change in k_{sn} diminishes with time as the high slopes developed by boulder-driven knickpoints relax. The t_{pbi} of R4 occurs after only 1 kyr and R4 never reaches the magnitude of the peak impact of hillslope-derived boulders (Figure 3a). k_{sn} is perturbed more in the megaflood boulder deposition case (R3) than our deposition scenarios with boulder bars composed of 4 m grains (R4) and hillslope-derived boulders (R2; Figure 3a).

Other landscapes experience the creation of knickpoints by landslide boulder deposits (e.g., Korup et al., 2006; Ouimet et al., 2007; Pratt-Sitaula et al., 2004). However, megaflood-deposited boulder bars are unique because of the regionally extensive/synchronous nature of these deposits and the ability of repeated megaflooding to refresh these deposits (i.e., deposit large boulders in the same locations during subsequent floods), leading to compounding effects. While the individual changes in bed elevation caused by each megaflood boulder bar (<4 m) are small relative to the total fluvial relief in our study area (~3,000 m), these small knickpoints occur everywhere a megaflood deposits groups of immobile boulders. The positions of these deposits within the flood pathway result from the interactions between megaflood hydraulics and the high-relief YSR valley topography (Morey et al., 2022). We posit that the spatial pattern of knickpoints produced by megaflood boulder deposition may depend more on valley-scale topography rather than either local stream power or hillslope stability. Because recurring megafloods of similar magnitude are likely to inundate the same features and deposit coarse boulders in the same positions in the landscape (Morey et al., 2022), there is a potential for a compounding effect of megaflood deposition. Figure 3b illustrates this effect for different recurrence intervals. If a flood has a recurrence interval shorter than t_{pbi} (2,500 years for our choice of model parameters), compounding effects of megaflood boulder deposition result in rapid change in average local k_{sn}. k_{sn} perturbations accrue at a slower rate for floods with recurrence intervals that are longer than t_{pbi} (Figure 3b), but still outpace the effects of hillslope-derived boulders provided that the recurrence interval is shorter than the time it takes for all megaflood boulders to decay—a point not reached in our experiments (i.e., >20 kyr).

19448007, 2024, 1, Downloaded from https://agupubs.onlinelibrary.wiley.com/doi/10.1029/2023GL105066, Wiley Online Library on [27/12/2023]. See the Terms and Conditions (https://onlinelibrary.wiley.com/terms-and-conditions) on Wiley Online Library for rules of use; OA articles are governed by the applicable Creative Commons License

Our results suggest that the depositional effects from a single megaflood could be felt for >20 kyr even with no subsequent megaflooding, but it is unlikely that, during past deglaciation, the eastern Himalaya went 20 kyr with only a single megaflood. In the eastern Himalaya, at least 3–8 megafloods likely occurred in the last 8–13 kyr (e.g., Borgohain et al., 2020; Liu et al., 2015; Montgomery et al., 2004; Panda et al., 2020; Song et al., 2013; Srivastava & Misra, 2012; Srivastava et al., 2017; Turzewski et al., 2020; Xu et al., 2020), suggesting that megaflood recurrence intervals might be short relative to the time required for rivers to process megaflood-derived boulders. The compound effects of megaflood deposition might therefore cause bedrock river valleys downstream of breached impounded lakes to retain the signature of megaflood deposition from past glacial/interglacial cycles. Our results illustrate the potentially long-lived legacy of megaflood deposition, with the caveat that megaflood erosion might also influence depositional perturbations to river form.

While our study focuses on megaflooding, any event that can cause repeated, regionally synchronous boulder deposition (i.e., earthquake-triggered landslides, seasonal flash flooding, etc., Dewey et al., 2021) could have similar geomorphic impacts. For example, large earthquakes can trigger landslides that deposit boulders synchronously and regionally in patterns unrelated to stream power (e.g., Devi & Bora, 2016; Meunier et al., 2007; Nowicki Jessee et al., 2018; Parkash, 2013). Earthquakes that recur in similar locations (i.e., on the same faults) could cause region-wide, repeated boulder deposition that could produce results similar to ours. Repeated landslide dam breach events at the same location have also been shown to cause widespread changes in channel slope (e.g., Korup et al., 2006; Li et al., 2022; Lin et al., 2022; L. Zhang et al., 2018; Q. Zhang et al., 2022). However, this change is tied to an event that impacts an individual location, creating a single knickpoint at the location of the landslide with effects diffusing downstream. The boulder deposition that occurs during repeated megafloods and/or large earthquakes is unique because it drives regional-scale geomorphic changes over several hundred kilometers.

Two potentially important complexities that our model does not address are the difference in deposit architecture between megaflood- and hillslope-derived boulder deposits and the impact of megaflood boulders deposited on hillslopes. Recent studies have found that individual particle placement (Yager et al., 2018) and the history of a deposit (Masteller et al., 2019) impact the entrainment threshold for particles. Because megaflood-derived boulder deposits are imbricated (Figure 1c), their entrainment threshold may be higher than if the same size grains were deposited by a landslide. Additional, the locations of greatest shear stress in an eastern Himalayan megaflood are not confined to the modern channel (Morey et al., 2022), but often occur on hillslopes, making it likely that megafloods also deposit boulders there (e.g., Clague et al., 2021). Boulder deposition on hillslopes could impede soil production, influencing the downslope transport of material (e.g., Glade et al., 2017; Shobe, Bennett, et al., 2021; Shobe, Turowski, et al., 2021), and blur the line between boulder sources as megaflood-derived boulders make their way into the valley bottom over time.

6. Conclusions

This study investigates the impact of widespread megaflood boulder deposition on bedrock river process and form. Inspired by documented megaflooding and observations of boulder bar deposits in the eastern Himalaya, we conduct model simulations that explore the geomorphic legacy of megaflood-derived boulders. Results show that, under our assumed boulder delivery dynamics and size distributions, the megaflood-deposited boulders initiate over 100 knickpoints with up to 3.5 m of relief each. Elevation change occurs at the locations of megaflood boulder bars; timescales of post-deposition knickpoint persistence depend on the river's ability to adjust to this influx of coarse sediment. Patterns of morphologic change produced by megaflood boulders are diagnostically different from those driven by hillslope-derived boulders. Given our assumptions and grain size observations, the deposition of boulders in bars during a single megaflood produces more change in channel steepness than do boulders supplied to the channel by hillslope processes responding to fluvial incision. Because megaflood boulder depositional patterns are dictated by valley-scale topography rather than modern fluvial hydraulics (Morey et al., 2022), if megafloods happen in rapid succession then the impact from boulder bar deposition might compound after each flood. Our results suggest that the modern YSR may still be experiencing the impacts of boulder bar deposition from the last sequence of megafloods and that it will continue to experience these effects for the next several thousand years, regardless of whether or not it experiences future megaflooding. Instantaneous, wide-spread, coarse boulder bar deposition from high-magnitude, low-frequency events like megafloods or earthquakes perturbs mountain landscapes, causing long-lasting geomorphic disequilibrium. Determining precisely

how this deposition impacts mountain landscapes helps us improve our holistic understanding of the legacy of geologically instantaneous events, one that is more complex than simply accounting for erosion.

Data Availability Statement

The model (longBRaKE) used in this study is available at Morey and Shobe (2023). Model results and boulder size data are available in the Supporting Material at Morey (2023).

Acknowledgments
We thank Jody Bourgeois, Cailey Condit, Juliet Crider, Paul Morgan, Michael Turzewski, all members of the University of Washington "Supergroup," and attendees of the 2023 GSA Penrose Conference on *The Role of Outburst Floods in Earth and Planetary Evolution* for insightful comments and suggestions on the development and presentation of this research. Monica Hill was an essential member of our field season in Arunachal Pradesh, which provided the basis for the boulder measurements upon which this work is built. Thanks to Oken Tayeng and Abor Travels for additional field support. Mattathias Needle trained AGJ to build the three-dimensional structure-from-motion (SfM) model of the boulder bar used to calibrate remote boulder measurements. We thank Julia Carr, Associate Editor Ivanov, and an anonymous reviewer for helpful reviews. Funding was provided by the Department of Earth and Space Sciences and the Quaternary Research Center at the University Washington, as well as the U.S. National Science Foundation (NSF EAR-2220336 and 1349279 to KWH, NSF EAR-2220335 to KAL, and NSF EAR-2220337 to CMS). The findings and conclusions in this publication are those of the authors and should not be construed to represent any official USDA or U.S. Government determination or policy.

References

Attal, M., Mudd, S. M., Hurst, M. D., Weinman, B., Yoo, K., & Naylor, M. (2015). Impact of change in erosion rate and landscape steepness on hillslope and fluvial sediments grain size in the Feather River basin (Sierra Nevada, California). *Earth Surface Dynamics*, *3*(1), 201–222. https://doi.org/10.5194/esurf-3-201-2015

Baker, V. R., & Kale, V. S. (1998). The role of extreme floods in shaping bedrock channels. *Geophysical Monograph-American Geophysical Union*, *107*, 153–166.

Baker, V. R., & Milton, D. J. (1974). Erosion by catastrophic floods on Mars and Earth. *Icarus*, *23*(1), 27–41. https://doi.org/10.1016/0019-1035(74)90101-8

Borgohain, B., Mathew, G., Chauhan, N., Jain, V., & Singhvi, A. K. (2020). Evidence of episodically accelerated denudation on the Namche Barwa massif by megafloods. *Quaternary Science Reviews*, *245*, 106410. https://doi.org/10.1016/j.quascirev.2020.106410

Bretz, J. H. (1925). The Spokane flood beyond the channeled scablands. *The Journal of Geology*, *33*(2), 97–115. https://doi.org/10.1086/623179

Clague, J. J., Roberts, N. J., Miller, B., Menounos, B., & Goehring, B. (2021). A huge flood in the fraser River valley, British Columbia, near the Pleistocene termination. *Geomorphology*, *374*, 107473. https://doi.org/10.1016/j.geomorph.2020.107473

Cook, K. L., Andermann, C., Gimbert, F., Adhikari, B. R., & Hovius, N. (2018). Glacial lake outburst floods as drivers of fluvial erosion in the Himalaya. *Science*, *362*(6410), 53–57. https://doi.org/10.1126/science.aat4981

Devi, R. K. M., & Bora, P. K. (2016). The impact of the great 1950 Assam earthquake on the frontal regions of the Northeast Himalaya. In *Earthquakes and their impact on society* (pp. 475–489).

Dewey, J. F., Goff, J., & Ryan, P. D. (2021). The origins of marine and non-marine boulder deposits: A brief review. *Natural Hazards*, *109*(2), 1981–2002. https://doi.org/10.1007/s11069-021-04906-3

Gilbert, G. K. (1890). *Lake Bonneville* (Vol. 1). United States Geological Survey.

Glade, R. C., Anderson, R. S., & Tucker, G. E. (2017). Block-controlled hillslope form and persistence of topography in rocky landscapes. *Geology*, *45*(4), 311–314. https://doi.org/10.1130/g38665.1

Hewitt, K. (1998). Catastrophic landslides and their effects on the Upper Indus streams, Karakoram Himalaya, northern Pakistan. *Geomorphology*, *26*(1–3), 47–80. https://doi.org/10.1016/s0169-555x(98)00051-8

Korup, O. (2006). Rock-slope failure and the river long profile. *Geology*, *34*(1), 45–48. https://doi.org/10.1130/g21959.1

Korup, O., Strom, A. L., & Weidinger, J. T. (2006). Fluvial response to large rock-slope failures: Examples from the Himalayas, the Tien Shan, and the Southern Alps in New Zealand. *Geomorphology*, *78*(1–2), 3–21. https://doi.org/10.1016/j.geomorph.2006.01.020

Lang, K. A., Huntington, K. W., Burmister, R., & Housen, B. (2016). Rapid exhumation of the eastern Himalayan syntaxis since the Late Miocene. *GSA Bulletin*, *128*(9–10), 1403–1422. https://doi.org/10.1130/B31419.1

Lang, K. A., Huntington, K. W., & Montgomery, D. R. (2013). Erosion of the Tsangpo Gorge by megafloods, eastern Himalaya. *Geology*, *41*(9), 1003–1006. https://doi.org/10.1130/G34693.1

Larsen, I. J., & Lamb, M. P. (2016). Progressive incision of the Channeled Scablands by outburst floods. *Nature*, *538*(7624), 229–232. https://doi.org/10.1038/nature19817

Li, W., Zhao, B., Xu, Q., Scaringi, G., Lu, H., & Huang, R. (2022). More frequent glacier-rock avalanches in Sedongpu gully are blocking the Yarlung Zangbo River in eastern Tibet. *Landslides*, *19*(3), 1–13. https://doi.org/10.1007/s10346-021-01798-z

Lin, Y., An, C., Parker, G., Liu, W., & Fu, X. (2022). Morphodynamics of bedrock-alluvial Rivers subsequent to landslide dam outburst floods. *Journal of Geophysical Research: Earth Surface*, *127*(9), e2022JF006605. https://doi.org/10.1029/2022JF006605

Liu, W., Lai, Z., Hu, K., Ge, Y., Cui, P., Zhang, X., & Liu, F. (2015). Age and extent of a giant glacial-dammed lake at Yarlung Tsangpo gorge in the Tibetan Plateau. *Geomorphology*, *246*, 370–376. https://doi.org/10.1016/j.geomorph.2015.06.034

Masteller, C. C., Finnegan, N. J., Turowski, J. M., Yager, E. M., & Rickenmann, D. (2019). History-dependent threshold for motion revealed by continuous bedload transport measurements in a steep mountain stream. *Geophysical Research Letters*, *46*(5), 2583–2591. https://doi.org/10.1029/2018gl081325

Meunier, P., Hovius, N., & Haines, A. J. (2007). Regional patterns of earthquake-triggered landslides and their relation to ground motion. *Geophysical Research Letters*, *34*(20), L20408. https://doi.org/10.1029/2007gl031337

Montgomery, D. R., Hallet, B., Yuping, L., Finnegan, N. J., Anders, A. M., Gillespie, A. R., & Greenberg, H. M. (2004). Evidence for Holocene megafloods down the tsangpo River gorge, southeastern tibet. *Quaternary Research*, *62*(2), 201–207. https://doi.org/10.1016/j.yqres.2004.06.008

Morey, S. M. (2023). Supplemental material for Morey et al. (2023) [Dataset]. Zenodo. https://doi.org/10.5281/zenodo.10246864

Morey, S. M., Huntington, K. W., Turzewski, M. D., Mangipudi, M., & Montgomery, D. R. (2022). The Erosional and depositional potential of Holocene Tibetan megafloods through the Yarlung Tsangpo Gorge, Eastern Himalaya: Insights from 2D hydraulic simulations. *Journal of Geophysical Research: Earth Surface*, *127*(5), 1–23. https://doi.org/10.1029/2021JF006498

Morey, S. M., & Shobe, C. M. (2023). smmorey/long-brake (V1.1.1) [Dataset]. Zenodo. https://doi.org/10.5281/zenodo.8056912

Nowicki Jessee, M. A., Hamburger, M. W., Allstadt, K., Wald, D. J., Robeson, S. M., Tanyas, H., et al. (2018). A global empirical model for near-real-time assessment of seismically induced landslides. *Journal of Geophysical Research: Earth Surface*, *123*(8), 1835–1859. https://doi.org/10.1029/2017JF004494

O'Connor, J. E., Clague, J. J., Walder, J. S., Manville, V., & Beebee, R. A. (2013). Outburst floods. In *Treatise on geomorphology* (Vol. 9). https://doi.org/10.1016/B978-0-12-374739-6.00251-7

Ouimet, W. B., Whipple, K. X., Royden, L. H., Sun, Z., & Chen, Z. (2007). The influence of large landslides on river incision in a transient landscape: Eastern margin of the Tibetan Plateau (Sichuan, China). *Geological Society of America Bulletin*, *119*(11–12), 1462–1476. https://doi.org/10.1130/b26136.1

19448007, 2024, 1, Downloaded from https://agupubs.onlinelibrary.wiley.com/doi/10.1029/2023GL105066, Wiley Online Library on [27/12/2023]. See the Terms and Conditions (https://onlinelibrary.wiley.com/terms-and-conditions) on Wiley Online Library for rules of use; OA articles are governed by the applicable Creative Commons License

Panda, S., Kumar, A., Das, S., Devrani, R., Rai, S., Prakash, K., & Srivastava, P. (2020). Chronology and sediment provenance of extreme floods of Siang River (Tsangpo-Brahmaputra River valley), northeast Himalaya. *Earth Surface Processes and Landforms*, *45*(11), 2495–2511. https://doi.org/10.1002/esp.4893

Parkash, S. (2013). Earthquake related landslides in the Indian Himalaya: Experiences from the past and implications for the future. In *Landslide science and practice: Volume 5: Complex environment* (pp. 327–334).

Pratt-Sitaula, B., Burbank, D. W., Heimsath, A., & Ojha, T. (2004). Landscape disequilibrium on 1000–10,000 year scales Marsyandi River, Nepal, central Himalaya. *Geomorphology*, *58*(1–4), 223–241. https://doi.org/10.1016/j.geomorph.2003.07.002

Scherler, D., DiBiase, R. A., Fisher, G. B., & Avouac, J. P. (2017). Testing monsoonal controls on bedrock river incision in the Himalaya and Eastern Tibet with a stochastic-threshold stream power model. *Journal of Geophysical Research: Earth Surface*, *122*(7), 1389–1429. https://doi.org/10.1002/2016JF004011

Schneider, J. M., Rickenmann, D., Turowski, J. M., Bunte, K., & Kirchner, J. W. (2015). Applicability of bed load transport models for mixed-size sediments in steep streams considering macro-roughness. *Water Resources Research*, *51*(7), 5260–5283. https://doi.org/10.1002/2014wr016417

Shobe, C. M., Bennett, G. L., Tucker, G. E., Roback, K., Miller, S. R., & Roering, J. J. (2021). Boulders as a lithologic control on river and landscape response to tectonic forcing at the Mendocino triple junction. *Geological Society of America Bulletin*, *133*(3–4), 647–662. https://doi.org/10.1130/b35385.1

Shobe, C. M., Tucker, G. E., & Anderson, R. S. (2016). Hillslope-derived blocks retard river incision. *Geophysical Research Letters*, *43*(10), 5070–5078. https://doi.org/10.1002/2016GL069262

Shobe, C. M., Tucker, G. E., & Rossi, M. W. (2018). Variable-threshold behavior in rivers arising from hillslope-derived blocks. *Journal of Geophysical Research: Earth Surface*, *123*(8), 1931–1957. https://doi.org/10.1029/2017JF004575

Shobe, C. M., Turowski, J. M., Nativ, R., Glade, R. C., Bennett, G. L., & Dini, B. (2021). The role of infrequently mobile boulders in modulating landscape evolution and geomorphic hazards. *Earth-Science Reviews*, *220*(January), 103717. https://doi.org/10.1016/j.earscirev.2021.103717

Sklar, L. S., & Dietrich, W. E. (2004). A mechanistic model for river incision into bedrock by saltating bed load. *Water Resources Research*, *40*(6), W06301. https://doi.org/10.1029/2003wr002496

Song, Z., Zhen-han, W., Xi-tao, Z., & Ke-yan, X. (2013). Glacial dammed lakes in the tsangpo River during late Pleistocene, southeastern tibet. *Quaternary International*, *298*, 114–122. https://doi.org/10.1016/j.quaint.2012.11.004

Srivastava, P., Kumar, A., Chaudhary, S., Meena, N., Sundriyal, Y. P., Rawat, S., et al. (2017). Paleofloods records in Himalaya. *Geomorphology*, *284*, 17–30. https://doi.org/10.1016/j.geomorph.2016.12.011

Srivastava, P., & Misra, D. K. (2012). Optically stimulated luminescence chronology of terrace sediments of Siang River, higher NE Himalaya: Comparison of Quartz and feldspar chronometers. *Journal of the Geological Society of India*, *79*(3), 252–258. https://doi.org/10.1007/s12594-012-0043-x

Turzewski, M. D., Huntington, K. W., & LeVeque, R. J. (2019). The geomorphic impact of outburst floods: Integrating numerical simulations, field and remote sensing observations of an extreme flood event in the eastern Himalaya. *Journal of Geophysical Research: Earth Surface*, *124*(5), 1056–1079. https://doi.org/10.1029/2018jf004778

Turzewski, M. D., Huntington, K. W., Licht, A., & Lang, K. A. (2020). Provenance and erosional impact of Quaternary megafloods through the Yarlung-Tsangpo Gorge from zircon U-Pb geochronology of flood deposits, eastern Himalaya. *Earth and Planetary Science Letters*, *535*, 116113. https://doi.org/10.1016/j.epsl.2020.116113

Wohl, E. E., & David, G. C. L. (2008). Consistency of scaling relations among bedrock and alluvial channels. *Journal of Geophysical Research*, *113*(F4), F04013. https://doi.org/10.1029/2008JF000989

Xu, Q., Ji, J., Zhong, D., Hu, Y., Deino, A., Chen, J., et al. (2020). Post-glacial entrenchment and knickpoint migration of the Yarlung tsangpo Gorge, southeastern Tibetan plateau. *Journal of Asian Earth Sciences*, *195*(March), 104337. https://doi.org/10.1016/j.jseaes.2020.104337

Yager, E. M., Schmeeckle, M. W., & Badoux, A. (2018). Resistance is not futile: Grain resistance controls on observed critical shields stress variations. *Journal of Geophysical Research: Earth Surface*, *123*(12), 3308–3322. https://doi.org/10.1029/2018jf004817

Zhang, L., Stark, C., Schumer, R., Kwang, J., Li, T., Fu, X., et al. (2018). The advective-diffusive morphodynamics of mixed bedrock-alluvial rivers subjected to spatiotemporally varying sediment supply. *Journal of Geophysical Research: Earth Surface*, *123*(8), 1731–1755. https://doi.org/10.1029/2017JF004431

Zhang, Q., Hu, K., Wei, L., & Liu, W. (2022). Rapid changes in fluvial morphology in response to the high-energy Yigong outburst flood in 2000: Integrating channel dynamics and flood hydraulics. *Journal of Hydrology*, *612*, 128199. https://doi.org/10.1016/j.jhydrol.2022.128199

References From the Supporting Information

Bernet, M., van der Beek, P., Pik, R., Huyghe, P., Mugnier, J.-L., Labrin, E., & Szulc, A. (2006). Miocene to Recent exhumation of the central Himalaya determined from combined detrital zircon fissiontrack and U/Pb analysis of Siwalik sediments, western Nepal. *Basin Research*, *18*(4), 393–412. https://doi.org/10.1111/j.1365-2117.2006.00303.x

Bunte, K., & Abt, S. R. (2001). Sampling frame for improving pebble count accuracy in coarse gravel-bed streams 1. *JAWRA Journal of the American Water Resources Association*, *37*(4), 1001–1014. https://doi.org/10.1111/j.1752-1688.2001.tb05528.x

Chirouze, F., Huyghe, P., van der Beek, P., Chauvel, C., Chakraborty, T., Dupont-Nivet, G., & Bernet, M. (2013). Tectonics, exhumation and drainage evolution of the eastern Himalaya since 13 Ma from detrital geochemistry and thermochronology, Kameng River section, Arunachal Pradesh. *Geological Society of America Bulletin*, *125*(3–4), 523–538. https://doi.org/10.1130/b30697.1

Ferguson, R. (2007). Flow resistance equations for gravel- and boulder-bed streams. *Water Resources Research*, *43*(5), W05427. https://doi.org/10.1029/2006WR005422

Finnegan, N. J., Hallet, B., Montgomery, D. R., Zeitler, P. K., Stone, J. O., Anders, A. M., & Yuping, L. (2008). Coupling of rock uplift and river incision in the Namche Barwa-Gyala Peri massif, Tibet. *Bulletin of the Geological Society of America*, *120*(1–2), 142–155. https://doi.org/10.1130/B26224.1

Howard, A. D. (1994). A detachment-limited model of drainage basin evolution. *Water Resources Research*, *30*(7), 2261–2285.

Howard, A. D., & Kerby, G. (1983). Channel changes in badlands. *Geological Society of America Bulletin*, *94*(6), 739–752. https://doi.org/10.1130/0016-7606(1983)94<739:ccib>2.0.co;2

Kean, J. W., & Smith, J. D. (2004). Flow and boundary shear stress in channels with woody bank vegetation. In S. J. Bennett & A. Simon (Eds.), *Riparian vegetation and fluvial geomorphology: Washington, D.C., American geophysical union, water science and application series* (pp. 237–252). https://doi.org/10.1029/008WSA17

Kean, J. W., & Smith, J. D. (2010). Calculation of stage-discharge relations for gravel bedded channels. *Journal of Geophysical Research*, *115*(F3), F03020. https://doi.org/10.1029/2009JF001398

19448007, 2024, 1, Downloaded from https://agupubs.onlinelibrary.wiley.com/doi/10.1029/2023GL105066, Wiley Online Library on [27/12/2023]. See the Terms and Conditions (https://onlinelibrary.wiley.com/terms-and-conditions) on Wiley Online Library for rules of use; OA articles are governed by the applicable Creative Commons License

Lamb, M. P., Finnegan, N. J., Scheingross, J. S., & Sklar, L. S. (2015). New insights into the mechanics of fluvial bedrock erosion through flume experiments and theory. *Geomorphology*, *244*, 33–55. https://doi.org/10.1016/j.geomorph.2015.03.003

Leopold, L. B., & Maddock, T. (1953). *The hydraulic geometry of stream channels and some physiographic implications* (Vol. 252). US Government Printing Office.

Rossi, M. W., Whipple, K. X., & Vivoni, E. R. (2016). Precipitation and evapotranspiration controls on daily runoff variability in the contiguous United States and Puerto Rico. *Journal of Geophysical Research: Earth Surface*, *121*(1), 128–145. https://doi.org/10.1002/2015jf003446

Smith, J. D. (2004). The role of riparian shrubs in preventing floodplain unraveling along the Clark fork of the Columbia River in the deer Lodge valley, Montana. In S. J. Bennett & A. Simon (Eds.), *Riparian vegetation and fluvial geomorphology: Washington, D.C., American geophysical union, water science and application series* (Vol. 8, pp. 71–85). https://doi.org/10.1029/008WSA06

Tucker, G. E. (2004). Drainage basin sensitivity to tectonic and climatic forcing: Implications of a stochastic model for the role of entrainment and erosion thresholds. *Earth Surface Processes and Landforms*, *29*(2), 185–205. https://doi.org/10.1002/esp.1020

Zeitler, P. K., Meltzer, A. S., Brown, L., Kidd, W. S., Lim, C., & Enkelmann, E. (2014). Tectonics and topographic evolution of Namche Barwa and the easternmost Lhasa block, tibet. In *Toward an improved understanding of uplift mechanisms and the elevation history of the Tibetan Plateau* (Vol. 507, pp. 23–58). Geological Society of America Special Papers.

19448007, 2024, 1, Downloaded from https://agupubs.onlinelibrary.wiley.com/doi/10.1029/2023GL105066, Wiley Online Library on [27/12/2023]. See the Terms and Conditions (https://onlinelibrary.wiley.com/terms-and-conditions) on Wiley Online Library for rules of use; OA articles are governed by the applicable Creative Commons License